

Application of a new magnetic helicity flux to disk galaxies

Luke Chamandy^{1*}, Ethan Vishniac², Sharanya Sur³ & Kandaswamy Subramanian¹
(Tentative)

¹Inter-University Centre for Astronomy and Astrophysics, Post Bag 4, Ganeshkhind, Pune 411007, India

²Department of Physics and Engineering Physics, University of Saskatchewan, 116 Science Place, Saskatoon, SK S7N 5E2, Canada

³School of Earth & Space Exploration, Arizona State University, P.O. Box: 876004 Temple, AZ 85287-6004, USA

17 August 2024

ABSTRACT

It is shown that application of the new small-scale magnetic helicity density flux of Vishniac (2012) to axisymmetric disk galaxies leads to several new effects not predicted by traditional mean-field galactic dynamo theory. The mean-field models used incorporate the dynamical α -quenching formalism as well as non-locality in time through the so-called τ effect. Notably, the flux leads to a magnetic α effect which grows the mean field to almost equipartition strength, even without any kinetic α effect being present. Moreover, the solution is oscillatory with period ~ 0.2 Gyr, which leads to the gradual buildup of multiple reversals of the field with galactocentric radius.

Key words: magnetic fields – MHD – dynamo – galaxies: magnetic fields – galaxies: spiral – galaxies: structure

1 INTRODUCTION

The theory of dynamical quenching has been instrumental in explaining how the mean-field dynamo need not fall prey to catastrophic quenching when magnetic helicity balance is included in the problem. The saviour is the helicity flux, which transports small-scale magnetic helicity density away from the dynamo active region, where its buildup would otherwise disable the traditional α -effect (Brandenburg & Subramanian 2005a; Subramanian & Brandenburg 2006). Such a model, when applied to realistic astrophysical scenarios, is able to naturally explain how large-scale magnetic fields are able to persist at near-equipartition levels, in the presence of say, an outflow that carries away small-scale helicity (Shukurov et al. 2006).

It has then been asked by several authors whether this newer, more complete picture provides more than just a convenient fix for the existing mean-field theory. There is evidence that, at least in magnetically dominated environments, it could, in fact, be the magnetic helicity that drives the large-scale dynamo, while the buildup of the kinetic helicity acts to quench it, rather than the other way around (Blackman & Field 2004; Brandenburg & Subramanian 2005b; Alexakis et al. 2006; Shapovalov & Vishniac 2011; Park & Blackman 2012).

In any case, one way in which progress can be made in mean field dynamo theory is for the flux of small-scale magnetic helicity density to be better unravelled. With this in mind, some authors have explored the nature of this flux

both analytically (Vishniac & Cho 2001; Subramanian & Brandenburg 2006; Vishniac 2012) and with direct numerical simulations (Brandenburg et al. 2009; Mitra et al. 2010). The most recent expression for the flux derived by Vishniac (2012) is especially interesting because it depends only on the presence of small-scale turbulence, comparably strong small-scale magnetic field and an overall rotation or shearing of the system—ingredients which are known to be present in many astrophysical objects. It is then interesting to apply this new flux to various astrophysical scenarios, and this is the aim of the present paper, where the focus is on disk galaxies. In Sect. 2 mean-field dynamo theory is briefly reviewed, in Sect. 3 the new flux is incorporated into galactic dynamo theory, and in Sect. 4 the numerical method is outlined. Section 5 contains a presentation of the results, while discussions and conclusions are given in Sect. 6.

2 MEAN FIELD DYNAMO THEORY

The dynamo (mean-field induction) equation is given by

$$\frac{\partial \bar{\mathbf{B}}}{\partial t} = \nabla \times (\bar{\mathbf{U}} \times \bar{\mathbf{B}} - \eta \nabla \times \bar{\mathbf{B}} + \mathcal{E}), \quad (1)$$

where $\mathbf{U} = \bar{\mathbf{U}} + \mathbf{u}$ and $\mathbf{B} = \bar{\mathbf{B}} + \mathbf{b}$. Here \mathbf{U} and \mathbf{B} are the velocity and magnetic fields, respectively, with \mathbf{u} and \mathbf{b} the fluctuating parts of those fields. An overbar indicates an ensemble average or volume average over scales larger than the turbulence but smaller than the system, and η is the microscopic (Ohmic) diffusivity. For isotropic, helical turbulence, the mean electromotive force (emf) is governed by the evolution equation (Kleeorin et al. 1996; Rogachevskii & Kleeorin

* E-mail: lchamandy@gmail.com

2000; Blackman & Field 2002; Rheinhardt & Brandenburg 2012),

$$\frac{\partial \mathcal{E}}{\partial t} = \frac{1}{\tau} (\alpha \bar{\mathbf{B}} - \eta_t \nabla \times \bar{\mathbf{B}} - \mathcal{E}), \quad (2)$$

where

$$\alpha = \alpha_k + \alpha_m = -\frac{1}{3} \tau_c \left[\mathbf{u} \cdot \nabla \times \mathbf{u} - \frac{1}{4\pi\rho} \mathbf{b} \cdot \nabla \times \mathbf{b} \right] \quad (3)$$

describes the so-called α effect (Parker 1955; Pouquet et al. 1976), and the turbulent diffusivity is given by

$$\eta_t = \frac{1}{3} \tau_c u^2 = \frac{1}{3} l u. \quad (4)$$

Here τ_c is the correlation time of the turbulence (assumed equal to the eddy turnover time, but see Shukurov 2004), u the rms value of \mathbf{u} , l the energy-carrying scale of the turbulence, and τ the dynamo relaxation time, which is assumed to be constant. In the $\tau \rightarrow 0$ limit, the familiar first order smoothing or quasilinear approximation (FOSA) is retrieved. The τ -effect thus generalizes the standard ($\tau \rightarrow 0$) prescription to allow for a finite response time of \mathcal{E} to variations in $\bar{\mathbf{B}}$ and the small-scale turbulence, and can be important in astrophysical scenarios (Hubbard & Brandenburg 2009; Chamandy et al. 2012).

The dynamics of α_m is determined by the helicity evolution equation (Subramanian & Brandenburg 2006),

$$\frac{\partial \chi}{\partial t} = -2\mathcal{E} \cdot \bar{\mathbf{B}} - 2\eta_t \mathbf{b} \cdot \nabla \times \mathbf{b} - \nabla \cdot \mathcal{F}, \quad (5)$$

where χ is the small-scale magnetic helicity density and \mathcal{F} is its flux. It is argued in Shukurov et al. (2006) that $\alpha_m = \eta_t \chi / (l^2 B_{eq}^2)$, and $\mathbf{b} \cdot \nabla \times \mathbf{b} = \chi / l^2$, where $B_{eq} \equiv \sqrt{4\pi\rho} u$ is the equipartition field strength. Using these relations, Eq. (5) can be rewritten as an evolution equation for α_m ,

$$\frac{\partial \alpha_m}{\partial t} = -\frac{2\eta_t}{l^2} \left(\frac{\mathcal{E} \cdot \bar{\mathbf{B}}}{B_{eq}^2} + \frac{\alpha_m}{\mathcal{R}_m} \right) - \frac{\eta_t}{l^2 B_{eq}^2} \nabla \cdot \mathcal{F}, \quad (6)$$

where the magnetic Reynolds number $\mathcal{R}_m \equiv \eta_t / \eta$. Making use of Eq. (4) and neglecting the Ohmic term since $\mathcal{R}_m \approx 10^{20} \gg 1$ for galaxies, we have

$$\frac{\partial \alpha_m}{\partial t} = -\frac{1}{36\pi\rho\eta_t} (2\mathcal{E} \cdot \bar{\mathbf{B}} + \nabla \cdot \mathcal{F}). \quad (7)$$

There are many possible contributions to \mathcal{F} (Subramanian & Brandenburg 2006). In general a flux of the form

$$\mathcal{F} = \mathcal{F}^{NV} + \mathcal{F}^a + \mathcal{F}^d \quad (8)$$

is considered. Here, the flux of Vishniac (2012) is referred to as the New Vishniac flux \mathcal{F}^{NV} to distinguish it from the Vishniac-Cho flux (Vishniac & Cho 2001). \mathcal{F}^{NV} is considered in more detail in Sect. 3. The advective flux

$$\mathcal{F}^a = \bar{\mathbf{U}} \cdot \nabla \chi \quad (9)$$

represents small-scale helicity being transported along with the mean flow. The phenomenologically-motivated diffusive flux

$$\mathcal{F}^d = -\kappa \nabla \chi, \quad (10)$$

seen in direct numerical simulations, may in fact arise due to the combined effect of more fundamental flux terms. Below, κ is generally set to zero, but finite κ is also considered in some models.

3 THE NEW VISHNIAC FLUX AND ITS APPLICATION TO DISK GALAXIES

The New Vishniac flux (Vishniac 2012) is given by

$$\mathcal{F}^{NV} = -\frac{\omega \tau_c^2 b^2}{3} \left[\left(\frac{2}{5} + \frac{11}{15} q \right) u^2 + \frac{13}{66} q \frac{b^2}{4\pi\rho} \right] \hat{z}, \quad (11)$$

where b is the rms value of the fluctuating part of the magnetic field, $\omega \hat{z}$ is the angular velocity and $q \equiv -d \ln \omega / d \ln r$. An important aspect of this flux is that it only requires the existence of fluctuating fields, which can easily arise for example by the action of a fluctuation dynamo. Note that unlike the Vishniac-Cho flux, the New Vishniac flux does not require a large-scale magnetic field, nor does it even require shear (so long as rotation is present, though in practice, the shear term is dominant in galaxies). Defining $\beta \equiv b^2 / B_{eq}^2$, we find

$$\mathcal{F}^{NV} = -4\pi\omega\rho\eta_t^2\beta \left(\frac{6}{5} + \frac{11}{5} q + \frac{13}{22} q\beta \right) \hat{z} = -16\pi f\omega\rho\eta_t^2\hat{z}, \quad (12)$$

where use has been made of Eq. (4), and where

$$f(q, \beta) \equiv \frac{\beta}{4} \left(\frac{6}{5} + \frac{11}{5} q + \frac{13}{22} q\beta \right).$$

Reasonable values for galaxies are $q = 1$ and $0.1 < \beta < 1$; $f(1, 1) \simeq 1$ and $f(1, 0.1) \simeq 0.09$.

Importantly, the New Vishniac flux was originally derived on the assumption that $\omega\tau_c \ll 1$. This assumption is usually acceptable for disk galaxies. For example, typical values $\tau_c = 10$ Myr and $\omega \approx 25 \text{ km s}^{-1} \text{ kpc}^{-1}$ gives $\omega\tau_c \approx 0.25$. However, $\omega\tau_c$ may be ≈ 1 for some galaxies, especially in the central regions; as this investigation is anyway approximate in nature, such complications are ignored.

To incorporate the New Vishniac flux (12) in a model for disk galaxies, one must ask how the quantities ω , ρ and η_t vary throughout the disk. What matters primarily for exploring the effects of the New Vishniac flux is the variation along \hat{z} , since the helicity flux enters as $\nabla \cdot \mathcal{F}$. It is known that the angular velocity ω decreases with distance from the galactic midplane, but slowly enough that it can safely be regarded as constant with height. On the other hand, variations in both the density ρ and turbulent diffusivity η_t may be important. The quantities u and l are also expected to depend only weakly on height within the disk, and for simplicity they are taken to be constant with height. This implies that η_t and τ_c are both constant with z . Note that β will also not vary with z , as it is assumed that $b^2 \propto \rho u^2 \propto B_{eq}^2$, and $\beta \equiv b^2 / B_{eq}^2$.

The vertical density profile may be simply modeled as a Gaussian (Ferrière 2001),

$$\rho = \rho_0 e^{-(z/h_\rho)^2}, \quad (13)$$

where z is the displacement from the midplane, ρ_0 and h_ρ are arbitrary functions of galactocentric radius and azimuth. LC: Note that I have not yet looked into buoyancy effects.

We may now calculate the term $-\nabla \cdot \mathcal{F} / (36\pi\rho\eta_t)$ of Eq. (7), using Eq. (12). Leaving aside the constant coefficient for now, we have

$$\frac{1}{\rho} \nabla \cdot (\rho \hat{z}) = \frac{1}{\rho} \frac{\partial \rho}{\partial z} = -\frac{2z}{h_\rho^2}, \quad (14)$$

Using Eqs. (7)-(10), (13) and (14), we find

$$\frac{\partial \alpha_m}{\partial t} = -\frac{2}{9} \left[\frac{\mathbf{E} \cdot \bar{\mathbf{B}}}{4\pi\rho_0\eta_t} e^{(z/h_\rho)^2} + \frac{4f\omega\eta_t}{h_\rho^2} z \right] - \nabla \cdot (\bar{\mathbf{U}}\alpha_m) + \kappa\nabla^2\alpha_m. \quad (15)$$

Defining $B_0 \equiv B_{eq}(0) = \sqrt{4\pi\rho_0}u$, and using this relation along with Eq. (4), Eq. (15) can be rewritten as

$$\frac{\partial \alpha_m}{\partial t} = -\frac{2}{3\tau_c} \left[\frac{\mathbf{E} \cdot \bar{\mathbf{B}}}{B_0^2} e^{(z/h_\rho)^2} + \left(\frac{2l}{3h_\rho} \right)^2 f\omega z \right] - \nabla \cdot (\bar{\mathbf{U}}\alpha_m) + \kappa\nabla^2\alpha_m. \quad (16)$$

Equations (1), (2) and (16) form a set of equations that can be solved to yield $\bar{\mathbf{B}}$, \mathbf{E} and α_m .

4 NUMERICAL TREATMENT

For simplicity, the disk and magnetic field are assumed to be axisymmetric; it is then convenient to use the ψ - T formalism (e.g. Mangalam & Subramanian 1994). Here, ψ is defined through the poloidal part of $\bar{\mathbf{B}}$, $\bar{B}_p \equiv (1/r)\nabla\psi \times \hat{\phi}$, and $T \equiv r\bar{B}_\phi$, where cylindrical polar coordinates (r, ϕ, z) are being used. Then $\bar{B}_r = -(1/r)\partial\psi/\partial z$, $\bar{B}_\phi = T/r$ and $\bar{B}_z = (1/r)\partial\psi/\partial r$. This formalism is easily generalized to the case $\tau \neq 0$, where, for convenience, we define $\mathbf{F} \equiv r\mathbf{E}$. We have allowed for the possibility of a finite mean vertical velocity flow \bar{U}_z , to model, e.g., a galactic fountain flow (Putman et al. 2012), but assume $\bar{U}_r = 0$ for simplicity. Likewise, η_t is taken to be constant throughout the disk. **LC: The equations below are general and do not assume that $\eta_t = \text{const}$. However they assume $\bar{U}_r = 0$ and $\partial\omega/\partial z = 0$.** Eqs. (1), (2) and (16) then become

$$\frac{\partial\psi}{\partial t} = -\bar{U}_z \frac{\partial\psi}{\partial z} + F_\phi, \quad (17)$$

$$\frac{\partial T}{\partial t} = q\omega \frac{\partial\psi}{\partial z} - \frac{\partial}{\partial z}(\bar{U}_z T) + \frac{\partial F_r}{\partial z} - \frac{\partial F_z}{\partial r} + \frac{F_z}{r}, \quad (18)$$

$$\frac{\partial F_r}{\partial t} = \frac{1}{\tau} \left(-\alpha \frac{\partial\psi}{\partial z} + \eta_t \frac{\partial T}{\partial z} - F_r \right), \quad (19)$$

$$\frac{\partial F_\phi}{\partial t} = \frac{1}{\tau} (\alpha T + \eta_t \Lambda^- \psi - F_\phi), \quad (20)$$

$$\frac{\partial F_z}{\partial t} = \frac{1}{\tau} \left(\alpha \frac{\partial\psi}{\partial r} - \eta_t \frac{\partial T}{\partial r} - F_z \right), \quad (21)$$

$$\begin{aligned} \frac{\partial \alpha_m}{\partial t} = & -\frac{2}{3\tau_c} \left[\left(-F_r \frac{\partial\psi}{\partial z} + F_\phi T + F_z \frac{\partial\psi}{\partial r} \right) \frac{e^{(z/h_\rho)^2}}{r^2 B_0^2} \right. \\ & \left. + \left(\frac{2l}{3h_\rho} \right)^2 f\omega z \right] - \frac{\partial}{\partial z}(\alpha_m \bar{U}_z) + \kappa \Lambda^+ \alpha_m, \end{aligned} \quad (22)$$

where $\Lambda^\pm \equiv \partial^2/\partial r^2 \pm (1/r)\partial/\partial r + \partial^2/\partial z^2$, $\alpha = \alpha_k + \alpha_m$ and Ohmic terms have been neglected.

For convenience, the following dimensionless quantities are defined:

$$R_\alpha \equiv \frac{\alpha_0 h}{\eta_t}, \quad R_\omega \equiv -\frac{q\omega h^2}{\eta_t}, \quad R_U \equiv \frac{U_0 h}{\eta_t}, \quad R_\kappa \equiv \frac{\kappa}{\eta_t}, \quad (23)$$

where α_0 and U_0 set the amplitude of the kinetic α effect and vertical mean velocity, respectively,

$$\alpha_k = \alpha_0 \tilde{\alpha}(z), \quad \bar{U}_z = U_0 \tilde{\bar{U}}_z(z), \quad (24)$$

Table 1. List of local 1D models presented in Fig. 1.

Model	R_ω	R_α	R_U	R_κ	τ/τ_c	f
1A	-20	0	0.45	0	1	1
1B	-20	0	1.16	0	1	1
1C	-30	0	0.45	0	1	1
1D	-20	4	0.45	0	1	1
1E	-20	0	0.45	0	2	1
1F	-20	0	0	0.3	1	1
1G	-20	1.5	0.45	0	1	0
1H	-20	0	0.45	0	1	0.34
2	–	0	0.45	0	0	1

and $\tilde{\alpha}$ and $\tilde{\bar{U}}_z$ are arbitrary dimensionless functions of z which are taken as

$$\tilde{\alpha} = \sin\left(\pi \frac{z}{h}\right), \quad \tilde{\bar{U}}_z = \frac{z}{h}. \quad (25)$$

Dimensionless units are employed such that lengths are measured in terms of the disk half-thickness h (assumed constant with radius), with the exception of radii, which are measured in units of the disk radius R . (This results in factors of $\lambda \equiv h/R$ multiplying some terms in the dimensionless equations.) Times are measured in terms of the characteristic vertical diffusion time at the midplane, $t_d = h^2/\eta_t$. In these units $\eta_t = h^2/t_d = 1$.

4.1 Local thin-slab models

Local models take the disk to be an infinite slab ($\partial/\partial r = 0$), except that $q = 1$ (flat rotation curve). Parameter values $l = 0.1$ kpc, $u = 10$ km s $^{-1}$, $h_\rho = h = 0.5$ kpc are adopted. The latter is an acceptable compromise between numerous results from observations and simulations (Ferrière 2001; Gaensler et al. 2008; Hill et al. 2012; Gent et al. 2012). This gives $t_d = 0.73$ Gyr, $\eta_t = 10^{26}$ cm 2 s $^{-1}$ and $\tau_c = t_d/75 = 10$ Myr. The mesh is linear and uses $n_z = 201$ grid points. Magnetic field is measured in units of B_0 , as defined above. The equations are solved with many combinations of parameters; models highlighted in Sect. 5 are listed in Tab. 1. Initial conditions are Gaussian random fields of dimensionless amplitude 10^{-2} for ψ and T , and zero for \mathbf{F} and α_m . Vacuum boundary conditions

$$\left. \frac{\partial\psi}{\partial z} \right|_{\pm h} = T(\pm h) = 0 \quad (26)$$

are employed (Ruzmaikin et al. 1988). For finite τ , $\partial T/\partial z$ must also be specified at $z = \pm h$, and is chosen to vanish there. **LC: Still studying the finite τ case.**

4.2 Global models

For global models ($\partial/\partial r \neq 0$), a Brandt rotation curve is adopted,

$$\omega = \frac{\omega_0}{(1+x^2)^{1/2}}, \quad (27)$$

where $x \equiv r/r_\omega$ and ω_0 and r_ω are parameters, so that with this profile, $\omega \rightarrow \text{const}$ as $x \rightarrow 0$ (solid body rotation) and $\omega \propto 1/r$ for $x \gg 1$ (flat rotation curve). The shear is determined by $q = x^2/(1+x^2)$. Values of l , u , h_ρ

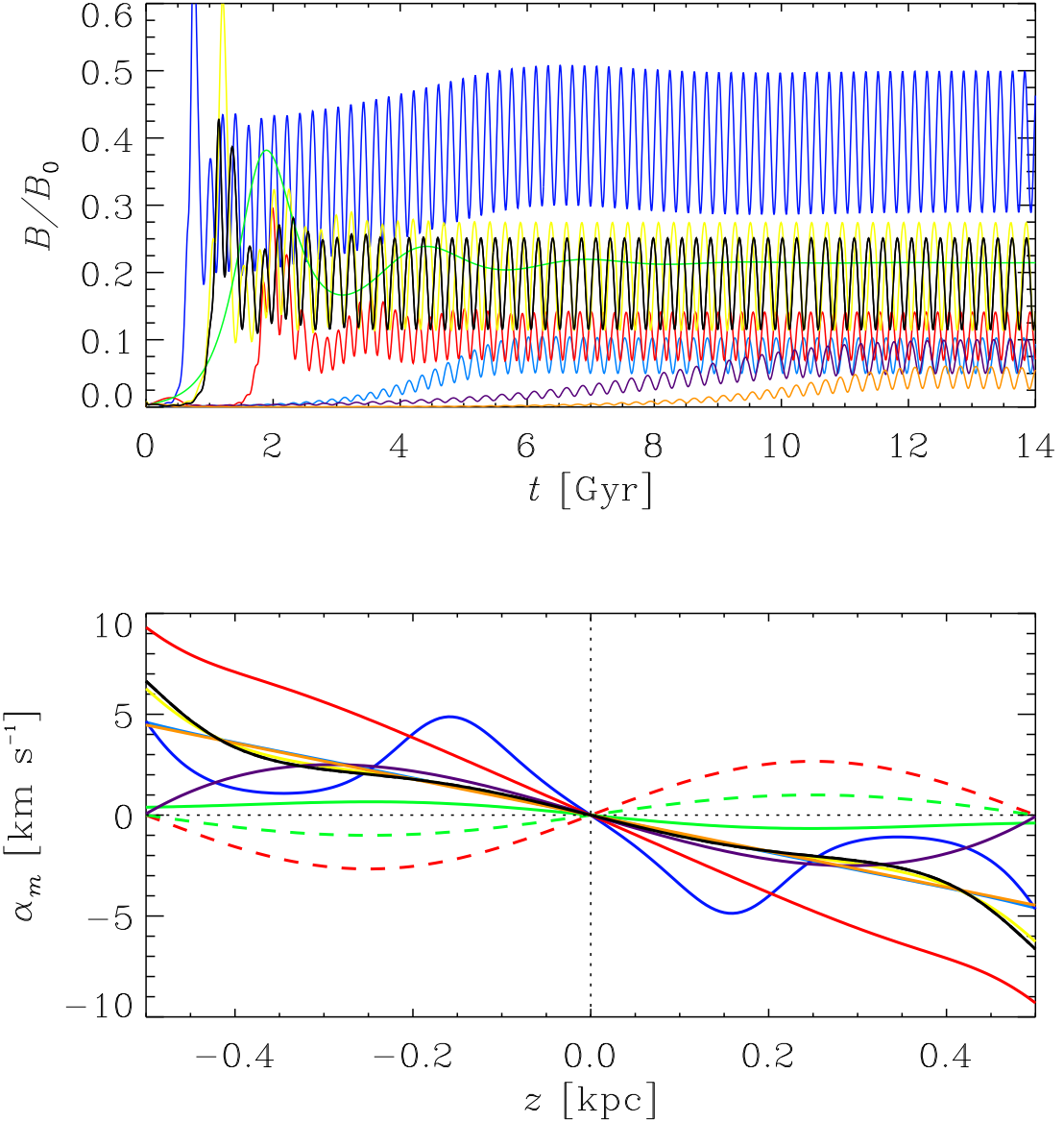


Figure 1. (a) Evolution of the field strength with time, and (b) α_m profile at $t = 12t_d = 8.8$ Gyr (with α_k dashed where finite), for Models 1A (black), 1B (light blue), 1C (blue), 1D (red), 1E (yellow), 1F (violet), 1G (green) and 1H (orange).

and h are as in the 1D models, all assumed to be independent of r for simplicity. The variation of the turbulent energy density with radius is modeled as an exponential, $B_0 = B_0(0)e^{-r/r_0}$, with r_0 a parameter (e.g., Beck 2007). Adopted values are $r_0 = R = 20$ kpc, $r_\omega = 0.1R = 2$ kpc, $\omega_0 = 76t_d^{-1} = 102$ km s\$^{-1}\$ kpc\$^{-1}. Otherwise, parameters are as listed in Model 2 of Tab. 1.

The mesh is linear in r and z with resolution $n_r = 401$, $n_z = 101$. The initial condition is $T = r^2(1 - r)e^{-r-z^2} \cos^2(\pi z/2)$, $\psi = \mathbf{F} = \alpha_m = 0$, though the solution at the times studied is not sensitive to the form of the seed magnetic field. Boundary conditions are

$$\psi = T = \frac{\partial\psi}{\partial r} = \frac{\partial T}{\partial r} = 0 \quad \text{at } r = 0, R \quad (28)$$

and

$$T = \frac{\partial\psi}{\partial z} = 0 \quad \text{at } z = \pm h. \quad (29)$$

5 RESULTS

5.1 Local solutions

LC: Note that for the 1D models, I have so far used a simpler code with variables \bar{B}_r and \bar{B}_ϕ , and there may be slight changes once the ψ - T code is used, though in theory the results should be identical. Properties of the solutions for the models of Tab. 1 are shown in Figs. 1–2. Fig. 1a shows the field strength, averaged over

z , as a function of time. In all 1D models listed in Tab. 1, a steady-state (saturated) solution is eventually reached. A finite R_U or R_κ is crucial to prevent α_m from building up at the disk boundaries; if both are zero, α_m grows to unphysical levels ($> u$) at the boundaries and a steady state is never reached.

For the fiducial model, Model 1A, parameters $R_\omega = -20$, $R_\alpha = 0$, $R_U = 0.45$, $R_\kappa = 0$, $\tau/\tau_c = 1$ and $f = 1$ are chosen. The chosen value of R_ω is fairly standard (Ruzmaikin et al. 1988), and is reasonable for the solar neighbourhood. Some disk galaxies are known to have outflows/galactic fountain flow, but outflow velocities may be highly variable in space, time, from one ISM component (e.g. hot, warm ionized) to another, and from one galaxy to another. Shukurov et al. (2006) estimates that the mass-weighted outflow speed for the ionized medium in which the magnetic field resides is $\sim 0.2 - 2 \text{ km s}^{-1}$, or $R_U = 0.3 - 3$. The value of unity chosen for τ/τ_c is arguably natural, and is supported by the results of direct numerical simulations (Brandenburg & Subramanian 2005b, 2007), though it depends on the details of the turbulence and may vary within galaxies and from one galaxy to another. The choice $f = 1$ is based on the optimistic estimate of equipartition of the small-scale magnetic field with the turbulence ($\beta = 1$), though smaller values of f are also considered below.

For Model 1a, the time-averaged value in the steady state is $0.19B_0$. This is comparable to the value $0.21B_0$ obtained for the traditional $\alpha^2\omega$ dynamo (Model 1G). On the other hand, the solution is oscillatory. This is expected given that $\alpha = \alpha_m$, whose sign is opposite to that of α_k in the traditional model. This case of oppositely signed α has been investigated previously for the accretion disk dynamo, and it was indeed found that the dominant solution is oscillatory (Brandenburg 1998; Brandenburg & Subramanian 2005a). The amplitude of the oscillations in the saturated state is $0.068B_0$ or 36% of the spatial and temporal average. The period is $0.31t_d = 0.23 \text{ Gyr}$.

Butterfly diagrams of \bar{B}_r , \bar{B}_ϕ and the field strength $\bar{B} = (\bar{B}_r^2 + \bar{B}_\phi^2)^{1/2}$ for Model 1A are shown in Fig. 2. The field has quadrupolar symmetry. Field initially grows at $z = 0$ and propagates away from the midplane with time. The magnetic energy is sometimes peaked at the midplane, and at other times away from it. The maximum magnitude of \bar{B}_r is only about half that of \bar{B}_ϕ . However, the magnetic pitch angle $p_B \equiv \tan^{-1}(\bar{B}_r/\bar{B}_\phi)$ is highly variable. Interestingly, the combined temporal-spatial average is -7° , which is in line with traditional estimates (Ruzmaikin et al. 1988).

5.1.1 Exploring the parameter space

The parameters of Tab. 1 can be varied and the corresponding variation in the solution examined. The rate of galactic shear/rotation is typically strongly variable with radius, and rotation curves differ substantially from one galaxy to another; therefore it is interesting to explore the effects of varying R_ω . The mean field strength in the steady state increases with $|R_\omega|$, and the dynamo needs less time to grow to the nonlinear stage. This is illustrated by the blue curve in Fig. 1a, for Model 1C ($R_\omega = -30$). Moreover, the period of the oscillations decreases but the amplitude increases as a result of increasing the magnitude of R_ω . These trends

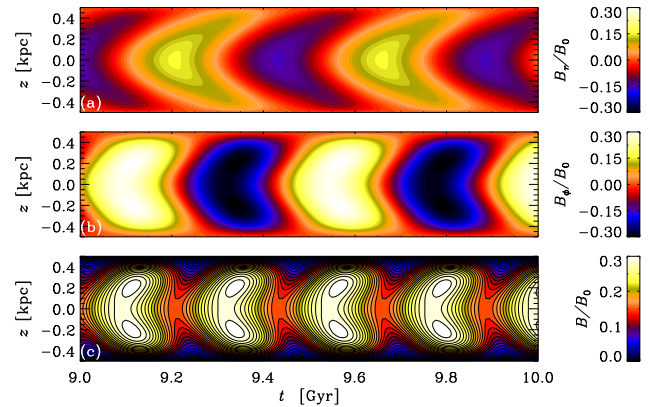


Figure 2. Butterfly diagrams showing the evolution of (a) \bar{B}_r , (b) \bar{B}_ϕ and (c) \bar{B} for Model 1A.

continue down to $R_\omega \approx -8$; for smaller values of $|R_\omega|$, the saturated field quickly becomes negligible.

The kinetic α effect is a key ingredient of the traditional galactic dynamo model, and is anyway thought to be important due to the presence of rotation and stratification. When the kinetic α effect is included by making R_α finite, the field grows to a higher level initially (within the first Gyr), but then decays before growing again to reach saturation, and the time-averaged steady-state field strength is smaller than for vanishing R_α . This is illustrated by the red curve of Fig. 1a for Model 1D ($R_\alpha = 4$). The period and amplitude of the oscillations both decrease with increasing R_α .

As mentioned above, R_U is difficult to constrain observationally, and various values of R_U were explored. The light blue curves of Fig. 1 illustrate properties of the solution for Model 1B, which uses a larger value of R_U than the fiducial model. It is found that the time-averaged magnetic field magnitude in the saturated state decreases with R_U , as might be expected, since more of the field is advected out of the disk. The amplitude of oscillations decreases with R_U while the period also decreases, but only weakly,

For $R_\kappa = 0.3$ (Mitra et al. 2010) and $R_U = 0$, a steady state is reached with a relatively weak time-averaged field strength $0.078B_0$, and amplitude equal to 33% of the mean, with α_m going to zero at the boundaries (Model 1F, violet in Fig. 1). If $R_\kappa = 0.1$, these numbers increase to $0.23B_0$ and 36%.

Changing the dynamo relaxation time τ also has a significant effect on the solution. As τ increases, the mean field strength in the steady state increase, as do the amplitude and period of the oscillations. This is illustrated by the yellow curve of Fig. 1a for Model 1E ($\tau = 2\tau_c$). These trends continue down to vanishing τ , with time-averaged field strength $0.18B_0$ and relative oscillation amplitude 32%, both smaller than in the fiducial model (1A), which uses $\tau/\tau_c = 1$.

Finally, fluctuating magnetic fields may be weaker than equipartition strength. Reducing the factor f in Eq. (12) (e.g. in Model 1H where it is reduced from unity to 0.34) leads to somewhat smaller saturation levels and absolute amplitude of the oscillations, and to slightly larger periods.

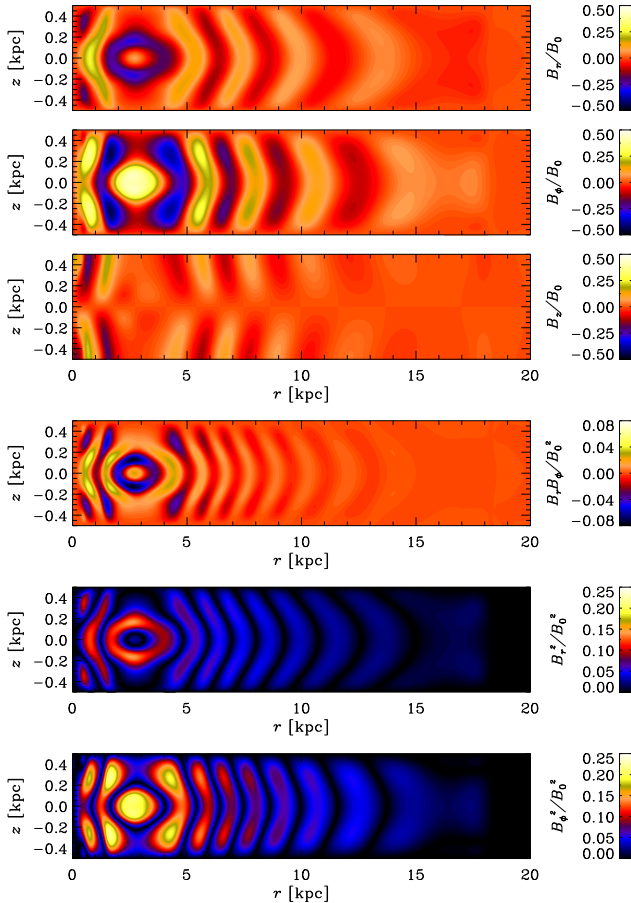


Figure 3. Snapshot of the field at $t = 3.65$ Gyr.

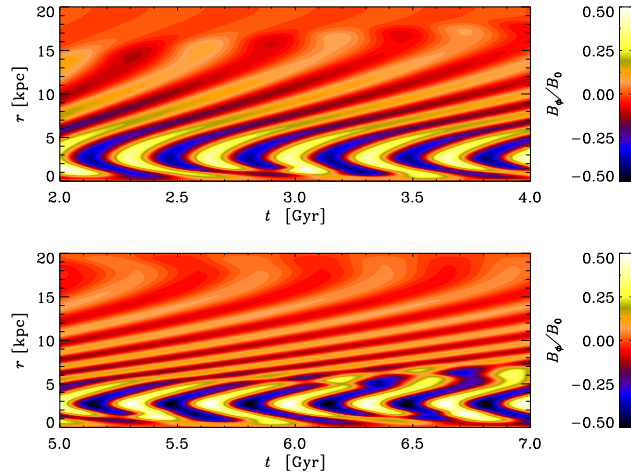


Figure 4. Butterfly diagrams showing the radial propagation of features in \bar{B}_ϕ at $z = 0$ for different temporal ranges.

5.2 Global solutions

The present study of global solutions is restricted to the case $\tau \rightarrow 0$ for simplicity. **LC: I am planning to illustrate the $\tau = \tau_c$ case instead, once the code is working perfectly for that case.** In Model 2, which is global and thus includes the radial direction, peaks of the field are observed

to propagate in radius as well as height. The time-averaged magnitudes of \bar{B}_r and \bar{B}_ϕ at the midplane peak just inside the radius at which the magnitude of R_ω is maximal. Features in the magnetic field seemingly propagate inward and outward from this point. Annuli of magnetic field, which alternate in sign along the radius, are gradually built up. Such annuli are clearly visible in snapshots of the field, one of which is shown in Fig. 3. Moving along radius, the pitch angle p_B varies over the full range -90° to 90° within each radial band; its volume average over the disk is $\langle p_B \rangle = -10^\circ$ for the snapshot shown. The value of $\langle p_B \rangle$ is usually negative with a temporal average of -6° .

The radial propagation is evident in butterfly diagrams with radius plotted along the y -axis, as in Fig. 4a, which shows the field at the midplane between $2 - 4$ Gyr (only the dominant \bar{B}_ϕ is shown to save space). Fig. 4b is the same except that the range is $5 - 7$ Gyr, and it can be seen that the annuli (at any given time) are now more numerous and closely spaced. The annuli continue to evolve in this fashion, and a steady state is not reached by $t = 15$ Gyr. Interestingly, however, the local period of the oscillations at any given radius remains more or less constant with time. **LC: More thought needs to be given to the results of 1D and 2D models!**

6 DISCUSSION AND CONCLUSIONS

The new small-scale magnetic helicity flux density of Vishniac (2012) has been applied to axisymmetric disk galaxies. It is argued that this New Vishniac flux, which operates in the presence of a substantial small-scale magnetic field along with rotation or shear, has dramatic effects on the galactic mean-field dynamo. For reasonable parameter values, its effect overwhelms that of the kinetic α effect traditionally appealed to in galactic dynamo theory. Most notably, the New Vishniac flux leads to oscillations of the mean field, multiple reversals in both components \bar{B}_r and \bar{B}_ϕ , and magnetic pitch angles that vary over the full range (-90° to 90°).

Such a picture presents quite a drastic change from the predictions of traditional mean-field theory (Ruzmaikin et al. 1988), and immediately begs the question: is it consistent with the observational literature? At first glance the answer seems to be 'no', but on inspection it might be argued that evidence for such an answer is not clear-cut. Oscillation time-scales of order 0.2 Gyr are rather long to have noticeable observational effects. Moreover, the occurrence of reversals in galaxies is still a matter of intense debate, with at least some authors claiming the existence of not just one, but several reversals in the Galaxy (Han 2012), though, admittedly, reversals in the large-scale field have yet to be observed in other galaxies (Beck 2012). Magnetic, pitch angle, meanwhile, is still rather poorly constrained observationally, especially at resolutions of hundreds of pc, at which strong variation occurs in the models.

It would be interesting to apply the New Vishniac flux to a non-axisymmetric galactic dynamo model, since the flux would tend to be larger within the spiral arms, where the small-scale magnetic field is known to be strongest. This may help to clarify the relationship between gaseous and magnetic spiral arms. It may be said that this work has also, albeit inadvertently, hinted at the possibility that the

new flux could be important in the solar context, where oscillations are known to play a central role.

REFERENCES

- Alexakis A., Mininni P. D., Pouquet A., 2006, ApJ, 640, 335
 Beck R., 2007, A&A, 470, 539
 Beck R., 2012, SSRv, 166, 215
 Blackman E. G., Field G. B., 2002, Physical Review Letters, 89, 265007
 Blackman E. G., Field G. B., 2004, Physics of Plasmas, 11, 3264
 Brandenburg A., 1998, in Abramowicz M. A., Bjornsson G., Pringle J. E., eds, Theory of Black Hole Accretion Disks Disc turbulence and viscosity. p. 61
 Brandenburg A., Candelaresi S., Chatterjee P., 2009, MNRAS, 398, 1414
 Brandenburg A., Subramanian K., 2005a, PhR, 417, 1
 Brandenburg A., Subramanian K., 2005b, A&A, 439, 835
 Brandenburg A., Subramanian K., 2007, Astronomische Nachrichten, 328, 507
 Chamandy L., Subramanian K., Shukurov A., 2012, MNRAS
 Ferrière K. M., 2001, Reviews of Modern Physics, 73, 1031
 Gaensler B. M., Madsen G. J., Chatterjee S., Mao S. A., 2008, PASA, 25, 184
 Gent F. A., Shukurov A., Fletcher A., Sarson G. R., Mantere M. J., 2012, ArXiv e-prints
 Han J., 2012, ArXiv e-prints
 Hill A. S., Joung M. R., Mac Low M.-M., Benjamin R. A., Haffner L. M., Klingenberg C., Waagan K., 2012, ApJ, 750, 104
 Hubbard A., Brandenburg A., 2009, ApJ, 706, 712
 Kleeorin N., Mond M., Rogachevskii I., 1996, A&A, 307, 293
 Mangalam A. V., Subramanian K., 1994, ApJ, 434, 509
 Mitra D., Candelaresi S., Chatterjee P., Tavakol R., Brandenburg A., 2010, Astronomische Nachrichten, 331, 130
 Park K., Blackman E. G., 2012, MNRAS, 423, 2120
 Parker E. N., 1955, ApJ, 122, 293
 Pouquet A., Frisch U., Leorat J., 1976, Journal of Fluid Mechanics, 77, 321
 Putman M. E., Peek J. E. G., Joung M. R., 2012, ARA&A, 50, 491
 Rheinhardt M., Brandenburg A., 2012, Astronomische Nachrichten, 333, 71
 Rogachevskii I., Kleeorin N., 2000, PRE, 61, 5202
 Ruzmaikin A. A., Shukurov A. M., Sokoloff D. D., 1988, Magnetic fields of galaxies. Kluwer, Dordrecht
 Shapovalov D. S., Vishniac E. T., 2011, ApJ, 738, 66
 Shukurov A., 2004, ArXiv e-prints
 Shukurov A., Sokoloff D., Subramanian K., Brandenburg A., 2006, A&A, 448, L33
 Subramanian K., Brandenburg A., 2006, ApJ, 648, L71
 Vishniac E. T., 2012, in American Astronomical Society Meeting Abstracts #220 Vol. 220 of American Astronomical Society Meeting Abstracts, A Simple Model for the Galactic Dynamo. p. 308.05
 Vishniac E. T., Cho J., 2001, ApJ, 550, 752